Indian Geotech J
https://doi.org/10.1007/s40098-024-01108-z

ORIGINAL PAPER

Shear Strength Characterization of the Interface Between Geocell Walls and Infill

J. C. V. Rezende[1] · **J. O. Avesani Neto**[1] · **J. G. Zornberg**[2]

Received: 26 April 2024 / Accepted: 3 November 2024

Abstract This study focuses on the evaluation of results from direct shear tests conducted to characterize the interface between geocell walls and various infill materials. Tests involved geocells from five different products, manufactured using high-density polyethylene (HDPE), novel polymeric alloy (NPA) and polypropylene (PP) nonwoven geotextiles. Two types of infill material (coarse and fine-grained soils) were adopted, along with different compaction conditions and grout to determine the interface shear strength under various conditions. The testing program also included varying the texture of the geocell walls as well as the number of perforations. Surface roughness profilometer tests were conducted to evaluate texture parameters. The analyses focused on the interface strength, obtained for both peak and post-peak conditions, characterized by the ratio between the interface friction angle and the soil peak friction angle. The results indicate that the presence of texture on the geocell wall led to comparatively high frictional efficiency, although the type of texturing was found not to have a significant effect on the frictional capacity of the geocells evaluated in this study. Additionally, the experimental results indicate that a perforation fraction of up to 10% of the total cell wall area did not significantly affect the interface shear strength. Based on the experimental program performed, a geocell with textured and perforated walls was found to lead to improved interaction with the infill material.

Keywords Geosynthetics · Geocell · Soil reinforcement · Shear strength · Interface friction angle · Wall roughness · Wall perforation

Introduction

Geocells are three-dimensional geosynthetics used in a wide range of geotechnical projects, including the stabilization of earth retaining walls, increase in foundations bearing capacity, protection of slopes from erosion, waterproofing of canals, protection of underground utilities and controlling permanent deflections in pavement systems [1–7]. In these applications, the proper selection of infill material and its interaction with the cell wall are crucial to optimize the system performance.

Over the past few decades, numerous laboratory tests have been conducted to evaluate the performance of geocell-reinforced soils. Some experiments have involved plate load tests to assess improvements in bearing capacity [8–12]. Other experimental studies have focused on embankments over soft soils, where geocells are used as basal reinforcement [13, 14]. Performance tests and analytical and computational modeling have also been conducted to quantify the geocell reinforcement performance; validate analytical models; and understand load support mechanisms for transportation infrastructure, such as railways and paved and unpaved roads [15–23]. Finally, experimental data have also been generated to quantify their performance in applications

✉ J. O. Avesani Neto
avesani@usp.br

J. C. V. Rezende
jcvrezende@gmail.com

J. G. Zornberg
zornberg@mail.utexas.edu

[1] Department of Structural and Geotechnical Engineering, Escola Politécnica at Universidade de São Paulo (EP-USP), São Paulo, SP, Brazil

[2] Department of Civil, Architectural and Environmental Engineering, The University of Texas at Austin, Austin, TX, USA

Published online: 20 November 2024

involving slope erosion protection, canals, retaining walls and underground utilities [24–28].

However, most of the tests have not directly quantified the interface shear strength between the different components of the system (i.e., between the geocell wall and the infill material), but have instead focused on evaluating the comparative performance between geocell-reinforced and unreinforced layers. In these configurations, researchers have used direct shear tests [29–31] or pullout tests [32–34] to quantify the interface shear strength between a geocell-reinforced layer and adjacent materials. However, there have been few studies aimed at characterizing the individual cells to determine the interface shear strength between the cell wall and the infill material.

Since the behavior of a geocell-reinforced soil layer (composite) is influenced by the mechanisms that develop within the geocell pockets, it is relevant to investigate the interaction between the fill material and cell wall. This interaction plays a significant role in various assumptions made in analytical and computational modeling for geocell-reinforced soil methodologies [35–37].

The present study aims at providing an overview of the interaction between infill materials and geocell walls under different conditions to enhance understanding of the interface shear strength characteristics. Direct shear (DS) tests were used to evaluate the interface between three fill materials and various commercially available geocells with different textures and perforation conditions. This paper presents the results and analysis of the interface shear strength between geocell walls and fill materials.

Materials

Geocell Walls

Five different geocell types from four different manufacturers were tested, as presented in Fig. 1. The geocell walls had different conditions, allowing for a comprehensive comparison and evaluation of the results.

The geocell walls involved different polymeric materials, which can be categorized into two groups: "rigid walls," such as high-density polyethylene (HDPE) and novel polymeric alloy (NPA), and flexible walls consisting of strips of polypropylene (PP) needle-punched nonwoven geotextile.

In addition to the polymeric material, the cell walls are also characterized by their surface roughness and the presence and pattern of perforations. A smooth HDPE geocell was manufactured for this study to allow evaluating the influence of roughness. Additionally, tests were conducted

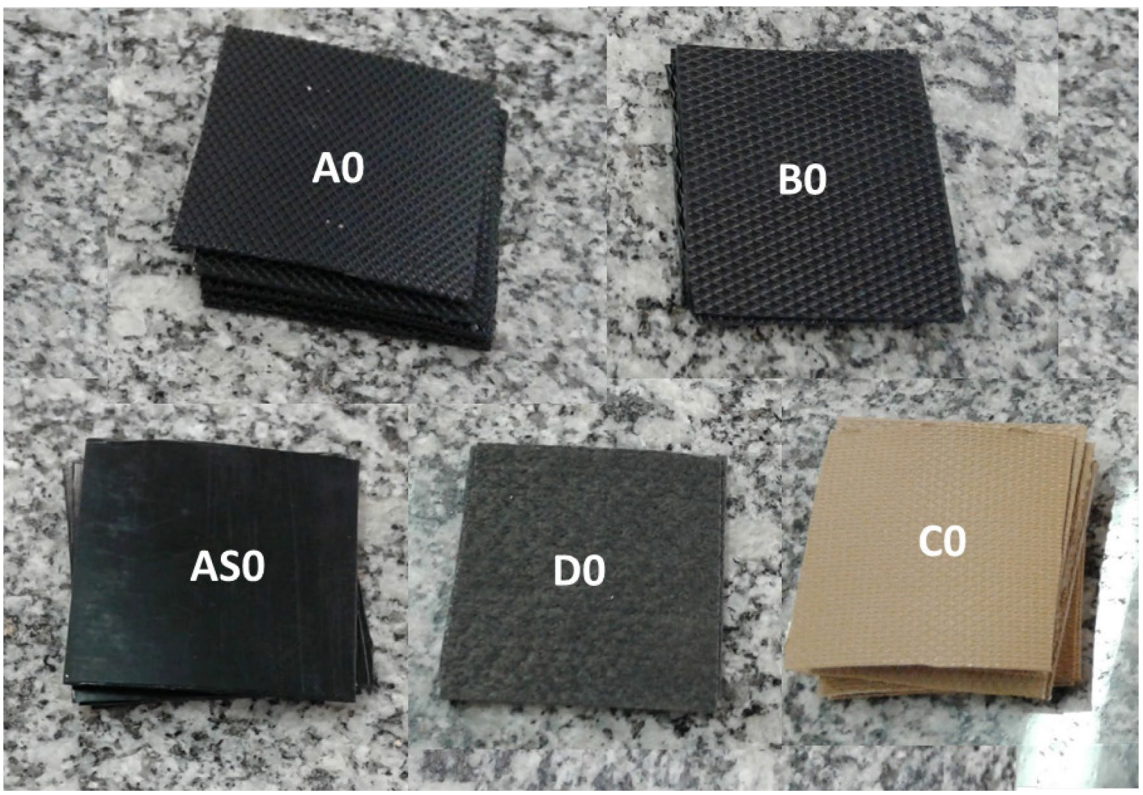

Fig. 1 Different geocell specimens without perforation used in the experiments

using an optical surface roughness profilometer to assess the surface roughness of each geocell.

Regarding cell wall perforations, a standard diameter of 10 mm has been adopted across manufacturers, with holes arranged in different patterns for each geocell. To assess the effect of this parameter, tests were conducted using different numbers of cell wall perforations as shown in Fig. 2. The perforation fraction was identified as a suitable parameter, which is defined as the ratio between the sum of the perforated areas and the cell wall area (A_h/A_w). The perforation fraction of geocells evaluated in this study ranged from 0 to 12%, although in commercially available geocells, this parameter ranges from 8 to 18%. The nonwoven geotextile strip (Geocell D) does not have factory perforations and was not evaluated in this parameter.

Table 1 provides details of the geocells tested in this study, followed by the nomenclature adopted herein. The geocell naming convention established for this study consists of a letter followed by a number. The letter refers to the type of geocell/texture/manufacturer (A, B, C and D for commercial geocells, and AS for the smooth HDPE geocell manufactured for this study for control purposes) and the number refers to the perforation fraction (0—no perforation, 6—6% perforation, etc.). For example, specimen B8 refers to a geocell from manufacturer "B" with 8% of perforation fraction. Table 1 also presents the peak and post-peak interface

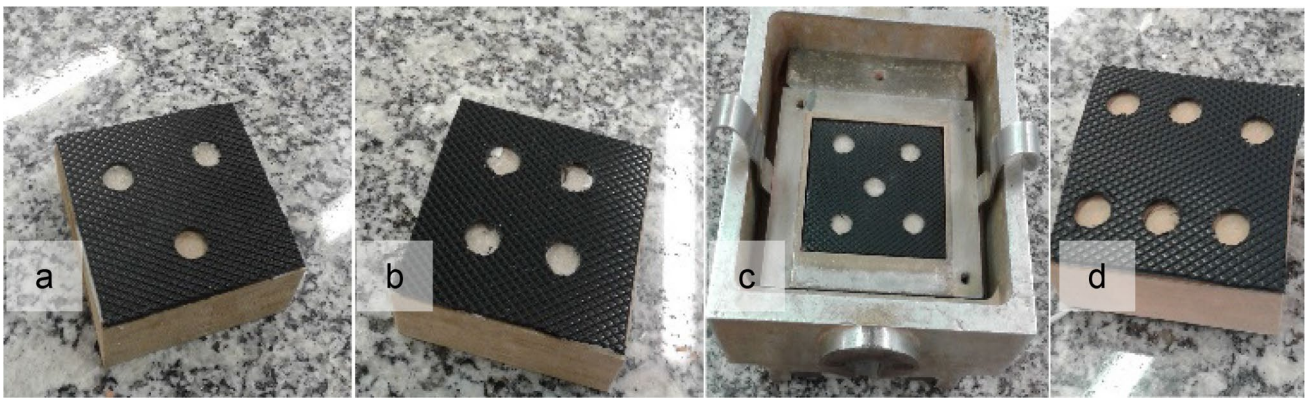

Fig. 2 Geocell A with perforation patterns: **a** 6%; **b** 8%; **c** 10%; and **d** 12%

Table 1 Scope of the testing program conducted in this study, including shear strength results

Geocell	Polymer	Roughness	A_h/A_w(%)	Soil 1		Soil 2		Grout	
				δ (°)	tanδ/tanφ	δ (°)	tanδ/tanφ	δ (°)	tanδ/tanφ
A0	HDPE	Textured	0	36.8	0.94	39.0	0.92	24.5	0.86
A6			6	36.7	0.94	–	–	–	–
A8			8	36.3	0.92	–	–	–	–
A10[a]			10	36.8	0.94	39.6	0.93	–	–
A12			12	34.4	0.86	–	–	–	–
AS0		Smooth	0	24.3	0.57	25.8	0.55	–	–
AS10			10	29.5	0.71	29.9	0.65	–	–
B0	HDPE	Textured	0	35.9	0.91	37.3	0.86	27.2	0.97
B8			8	35.2	0.89	–	–	–	–
B12[a]			12	32.8	0.81	36.9	0.85	–	–
C0	NPA	Textured	0	35.3	0.89	37.1	0.85	21.3	0.74
C10[a]			10	34.5	0.87	36.9	0.85	–	–
D0[a]	PP nonwoven geotextile	[b]	0	34.3	0.86	36.4	0.83	20.4	0.70
D8			8	35.6	0.90	–	–	–	–
D10			10	37.0	0.95	–	–	–	–

HDPE, High-density polyethylene; PP, polypropylene; NPA, novel polymeric alloy; A_h, sum of perforated cell wall area; A_w, cell wall area

[a]Normal condition of the manufactured geocell

[b]Roughness inherent to nonwoven geotextiles

friction angles obtained from the experiments—which are discussed in Sect. "Results and Discussion."

Infill Soils

Two types of infill soil were utilized to assess the interface shear strength with the different geocells. The first type, referred to as soil 1, is sand known as "normal Brazilian sand" [38]. This material was used in its dry state and compacted to its maximum relative density (minimum void ratio) to represent typical conditions in reinforcement applications, whereby granular materials are commonly used, and high energies are required to meet stability and deformability design criteria. Figure 3 presents its particle size distribution, which is characterized by a coefficient of uniformity (C_u) of 1.81, coefficient of curvature (C_c) of 1.18, effective particle size of 0.13 mm and specific gravity of 2.74. The minimum and maximum void ratios found were equal to 0.61 and 0.82, respectively. This soil classifies as a poorly graded sand (SP) according to the unified soil classification system (USCS) and as an A3 soil according to the classification system of the highway research board (HRB).

The second type of soil, referred to as soil 2, is a soil with a comparatively high fines content involving a typical Brazilian lateritic natural soil. This soil has been commonly used to fill geocells in erosion protection applications, whereby compaction control is usually not implemented, and the development of vegetation is desired. Therefore, a comparatively small degree of soil compaction was applied to this soil during testing. Soil 2 fines content exceeded 50%. Figure 3 depicts the particle size distribution curves obtained using two different procedures: one with a dispersing agent (hexametaphosphate) and the other without it (referred to as soil 2* in the figure). The soil liquid limit (LL), plastic limit (PL), plasticity index (PI) and specific gravity were determined as 39, 29, 10 and 2.67, respectively. According to the USCS, soil 2 classifies as a low-plasticity silt (ML). According to the HRB classification system, it falls under category A4. Without the dispersing agent, the soil classifies as an SM and A4 based on the USCS and HRB classification system, respectively.

Grout

In addition to the two soils, grout was also utilized to assess the interface shear strength with the different geocells to understand the trends when a geocell is filled with cementitious materials, such as concrete, which is common in hydraulic projects such as canals. To prevent the result from being affected by the local influence caused by aggregates, grout rather than concrete was chosen because of the comparatively small dimensions of the shear box. Without coarse components like gravel, note that the use of grout, which lacks coarse materials, in these tests would conservatively represent a lower bound of the geocell interface shear strength involving cementitious materials. The specimens were prepared using a mixture of 300 g water, 500 g cement and 1,500 g sand, resulting in a water–cement (*w/c*) ratio of 0.6, to which a proportion of 1:3.5 g of superplasticizer additive for concrete (ADVA CAST 525) was added. The blocks were cured for approximately one month, resulting in a compressive strength of 7.4 MPa.

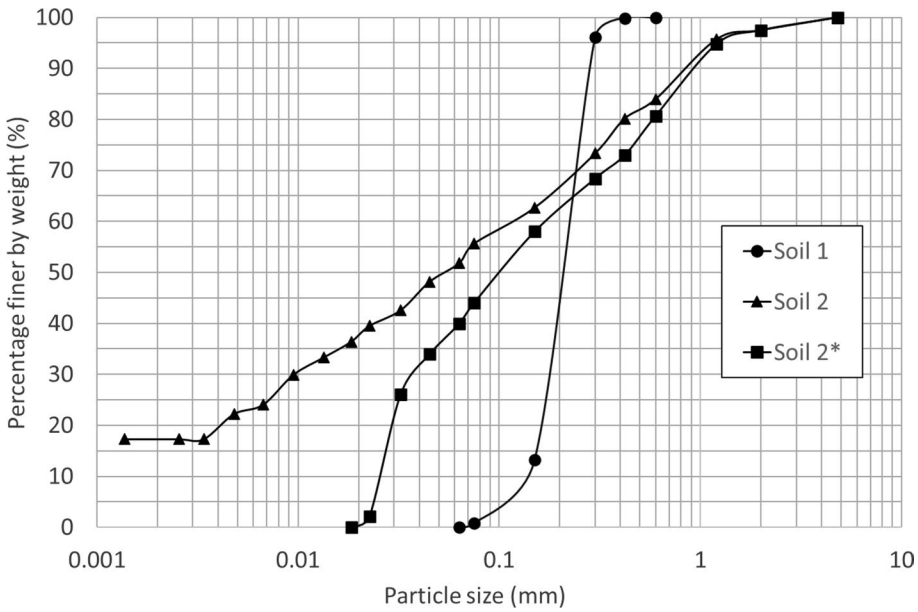

Fig. 3 Soil particle size distribution

Laboratory Test Model

Testing Apparatus

A conventional direct shear (DS) apparatus, consisting of a fixed lower box and free upper box for shearing, was used in this investigation. Considering that the height of geocells used in various geotechnical applications typically ranges from 50 to 200 mm, which is consistent with the standard dimensions of commercially available geocells, the shear box used had dimensions of 60 × 60 mm in length and width (36 cm^2 area) and 50 mm in height, resulting in an internal volume of 180 cm^3. The horizontal and vertical displacements, and applied force were measured during testing, allowing for determining volumetric and horizontal strains as well as shear stress.

Test Procedures and Variables

Tests were conducted following the procedure provided in ASTM D3080 at a shear displacement rate of 0.267 mm/min. Three different normal stresses of 50 kPa, 100 kPa and 200 kPa were applied in each test. The tests were conducted following a procedure similar to the one described in [40]. The tests for interface shear strength characterization were performed by securing the geocell walls to a wooden block with dimensions similar to those of the DS test boxes. This block was then placed in the lower DS test box, while the upper box was filled with soil or grout. For soils 1 and 2, compaction was employed during the fill process, aiming for a specified mass target as elaborated in the following section. In instances involving geocell walls with perforations, soils were allowed to fill these openings. Since the grout was used in the form of precast blocks, perforated geocell walls were not employed in this interface, as the openings could not be filled with grout in the precast block circumstance.

The methodology to report the test results was similar to previous research [41–43] in terms of peak and large-displacement interface friction angle, respectively, δ and δ_{ld}. The large-displacement interface friction angle was defined as a horizontal displacement of 8 mm. The results are reported in terms of the peak interface friction angle (δ) and the ratio between the tangents of peak interface friction angle and the soil peak friction angle ($\tan\delta/\tan\varphi$) here named as "interface friction efficiency" for convenience.

Internal Shear Strength Characterization of Soils and Grout

The soils adopted in this testing program were prepared for different initial conditions in the DS box used in tests to determine both the internal and interface friction angles. Soil 1, consisting of a coarse material typically used to fill geocells in reinforcement applications, was compacted to a comparatively high density to represent conditions typical of reinforcement and stiffening applications. The initial relative density condition of soil 1 was 100%, corresponding to a unit weight of 17.3 kN/m^3. The relative density was achieved by controlling the mass of the material placed in the upper box to achieve the minimum void ratio of the sand. The peak friction angle of the dry sand at this relative density was determined to be 38.5° through standard DS tests following the procedure described above, as shown in Figs. 4 and 5. Figure 4 depicts the shear stress and displacement from the DS for soil 1 (squares patterns), showing that this soil exhibits a clear peak at 2.0 mm of shear displacement, particularly for normal stresses of 100 and 200 kPa. The shear strengths and failure envelopes were determined by analyzing the maximum stresses obtained as depicted in Fig. 5. Considering no cohesion intercept (dry sand), where a R^2 equal of 0.998, the failure envelope for soil 1 was obtained. The post-peak friction angle was determined as 33.3° ($\varphi_{pp}/\varphi = 0.86$).

Soil 2 primarily consists of fine particles and is commonly used to fill geocells in erosion control applications, particularly in slopes, associated with vegetation. Achieving a high degree of soil compaction during construction is challenging in these scenarios due to difficulties in filling, installing and compacting the soil. To represent this field condition, a degree of soil compaction of 85% (standard Proctor) was maintained in all tests, resulting in an average soil unit weight of 15.1 kN/m^3 and moisture

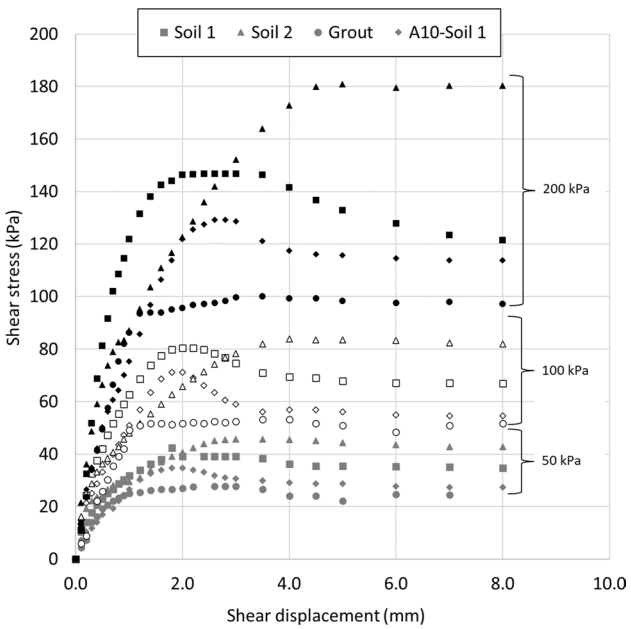

Fig. 4 Shear stress–displacement behavior of soils 1 and 2, grout and Geocell A10–soil 1 interface

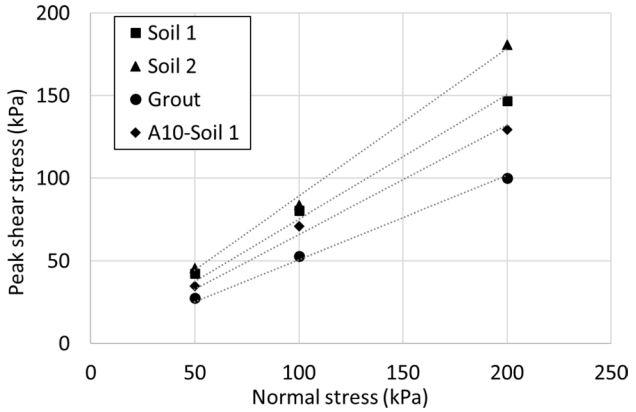

Fig. 5 Peak shear strength of soils 1 and 2, grout and Geocell A10–soil 1 interface

content of 1.89%. The degree of soil compaction was controlled using the same method as for soil 1. Using triangle patterns, Fig. 4 shows the shear stress and displacement for soil 2, in which practically no peak was obtained, due to the light compaction situation. Also, the maximum shear strength value for soil 2 was obtained at displacements ranging from approximately 4–5 mm. Figure 5 presents the failure envelope, again considering no cohesion intercept due to the dry and compaction situations, where an R^2 equal to 0.999 was calculated. The φ and (φ_{pp}) were determined via standard DS tests as 41.5° and 40.7°, respectively (Fig. 5). The ratio φ_{pp}/φ was found to be 0.98. The friction angle value obtained for soil 2 may be considered high for typical soils classified as ML. The values obtained in this investigation are consistent with those reported in previous studies involving lateritic and residual tropical soils. [44–52].

In the case of grout, the interface shear strength of the joint was determined. Two grout blocks were placed in the DS box to determine the peak and post-peak interface friction angle of the joint—here also termed as φ and φ_{pp} for convenience. The grout blocks DS tests were conducted under confining stresses of 50, 100 and 200 kPa. According to Figs. 4 and 5 (circle patterns), the maximum shear strength for the grout was reached at displacement values of 2 to 3 mm. The peak and post-peak friction angles in the joint between the blocks were determined to be 27.9° and 26.3°, respectively (ratio φ_{pp}/φ equal to 0.94).

Table 2 Roughness parameters as obtained by optical profilometer

Geocell	R_c (μm)	R_t (μm)	R_a (μm)
A	41.2	94.6	10.3
AS	16.6	31.0	2.3
B	34.4	56.4	7.4
C	66.3	153.5	22.9
D	64.9	127.0	19.6

R_c: Mean height of the profile

R_t: Total height of the profile

R_a: Arithmetical mean deviation of the profile

Results and Discussion

This section briefly shows and discusses profilometer results, interface shear strength results and its influence factors such as infill materials, wall texturization and perforation.

Profilometer Tests to Quantify Geocell Wall Roughness

The results from an optical profilometer to quantify the roughness parameters [43, 53, 54] are described in this section. The testing program involved conducting a series of three roughness measurements for each geocell sample. These measurements were used to create a roughness profile of the most representative section of the geocell wall samples. The measurements were taken in portions of the geocell walls without perforations. Three parameters obtained from the profilometer were associated with the surface roughness [43, 54, 55]: i. total height of the profile (R_t), which is obtained from the maximum peak to valley height in the tested profile; ii. the mean height of the profile (R_c); and iii. the arithmetic mean deviation of the profile (R_a).

The equipment used was a Taylor Hobson CCI optical profilometer, with high sensitivity and an accurate detector to allow determining the position and estimating the superficial height of this point, regardless of the surface texture. For each test, the three roughness parameters and 3D profiles of the samples were obtained. The optical profilometer captured three sections of each specimen measuring 1600×1600 μm^2 via a lens with $10\times$ magnification. A wavelength cutoff of 0.1 μm was specified. A qualitative–quantitative analysis was conducted using the three parameters, focusing on the relationship among the results of different geocells rather than analyzing the absolute values obtained. Table 2 presents the three parameters calculated by the profilometer.

In Table 2, the smooth geocell (AS) produced the lowest results across parameters measured with the profilometer, with values at least less than 50% of those for the other geocells. Geocell AS absence of surface textures yielded a significant decrease in surface roughness, which could be observed qualitatively by handling the sample and

quantitatively using the profilometer. The texture patterns of Geocells C and A exhibited the best performance based on profilometer measurements for the "rigid wall" group. Geocell C had higher values for all parameters, which were approximately 50% to 100% higher than those obtained for Geocell A. Geocell B, in turn, had the lowest performance among the geocells with "rigid walls" and produced the lowest parameter values, ranging from about 60% to 30% of those for the other geocells.

Lastly, Geocell D, manufactured using geotextile strips, produced high values in all the parameters measured by the profilometer, very similarly to the values obtained for Geocell C. This may be attributed to the surface roughness of the nonwoven geotextile resulting from the needling process used in its manufacture. Unlike extruded materials, such as HDPE and NPA, which require a texturing process, the surface of a needled geotextile exhibits comparatively high roughness due to the presence of PP polymer filaments.

Interface Shear Strength Results

A total of 108 DS tests were conducted, categorized into 36 test series with three different normal stresses. The experiments included fill materials, such as soils and grout (9 tests in 3 series), geocell wall interface tests in various configurations (84 experiments in 28 series) and repetitions of several tests to assess repeatability (15 experiments in 5 series). Table 1 provides a summary of all the interface shear tests conducted, excluding tests solely involving soils and grout, and repetitions that yielded consistent results.

In addition to the DS test results corresponding to the internal shear strength of the different materials, as mentioned in Sect. "Internal Shear Strength Characterization of Soils and Grout," the results in Fig. 4 also show the interface shear stress versus shear displacement curves from DS tests conducted to characterize the Geocell A10–soil 1 interface. Among the multiple interfaces investigated in this study, Geocell A10–soil 1 interface is adopted in this section to illustrate the general behavior observed in the testing program. As shown in Fig. 4, Geocell A10–soil 1 interface (represented by diamond patterns) exhibits a well-defined peak shear strength, which was reached at relatively small displacements of approximately 2 mm, in the same behavior previously noted to soil 1 (Sect. "Internal Shear Strength Characterization of Soils and Grout"). The figure shows that the shear stress obtained for soil 1 at any given shear displacement, including the peak shear strength, was consistently higher than that obtained for the Geocell A10–soil 1 interface. This behavior was consistent with other geocells and interfaces as well.

As previously remarked for the infill soils and grout (Sect. "Internal Shear Strength Characterization of Soils and Grout"), the Geocell A10–soil 1 interface failure envelope (Fig. 5) also shows that the peak shear strength data can be represented by a linear shear strength envelope, where R^2 equal to 0.998 was obtained for this interface.

Based on the results in Table 1, the textured rigid wall geocells (A, B and C) and nonwoven geotextile geocell (D) were observed to reached the following peak interface friction angles (δ): 33° to 37°, with an average of 35.5°, for soil 1; 36° to 39°, with an average of 38°, for soil 2; and 20° to 27°, with an average of 23.4°, for grout. These values indicate that the geocell walls may provide a significant surface interaction for the different materials tested in this study as they reach interface friction angles that are very close to the internal friction angles (φ) of the soils. Overall, the interface friction efficiency ($\tan\delta/\tan\varphi$) exceeded 0.8—and was often higher than 0.9.

In contrast, non-textured Geocell AS exhibited interface friction angle values significantly lower than the soil friction angles. These values ranged from 24° to 30° and were the lowest values observed in tests conducted in geocell walls without perforations. The resulting $\tan\delta/\tan\varphi$ values range from 0.55 to 0.71, indicating a comparatively low interface frictional efficiency for the materials and conditions examined in this study.

While tests to determine the interface shear strength of geocell walls against different infill materials are not commonly found in the literature, test results for interfaces involving geomembranes and geotextiles have been reported in several previous studies. Although the texturing patterns are generally tailored for geocell applications, the materials used in geocell walls are often similar to those used in geomembranes (HDPE) and nonwoven geotextiles (PP). A comparison of results reported in several studies [43, 54, 56–65] reveals that the peak interface friction angles obtained herein are similar in magnitude to those reported in the literature for applications other than geocells.

The influence of the fill material, tested using geocell walls without perforations, was evaluated for all the geocell walls tested in this research. Table 1 presents the results of interface shear tests conducted using the various fill materials. In addition, Fig. 6 summarizes the interface friction efficiency ($\tan\delta/\tan\varphi$) for all geocell wall samples in non-perforated surface conditions.

Although soil 2 had a higher internal friction angle than soil 1, the evaluation of results presented in Fig. 6 reveals that interface shear tests involving soil 1 led to higher efficiency values than soil 2. This trend is consistent with previous studies, indicating that coarse soils have greater frictional efficiency than silty and clayed soils when interacting with other geosynthetics [66, 67]. Additionally, the high compaction energy in tests on soil 1 facilitated increased contact with the geocell wall, potentially contributing to increasing its efficiency when compared to soil 2 and its reduced compaction energy in testing. Apart from Geocell

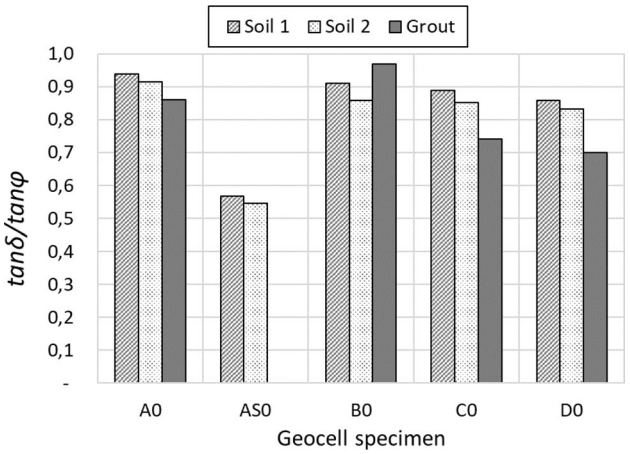

Fig. 6 Influence of fill material and roughness pattern on tanδ/tanφ ratio

B, the tanδ/tanφ ratio for the grout interface was lower than those obtained for the two soils. This may be attributed to the smoother texture of the grout surface, which reduces frictional efficiency.

As previously mentioned, the results in Fig. 6 show that the presence of texture significantly increases the efficiency of the fill material–cell wall interaction. For the same sample (Geocell A), which was evaluated textured and smooth, specifically for this study, both soils exhibited an approximately 50% increase in performance in the tanδ/tanφ ratio due to the presence of texture in the absence of perforations.

Table 2 and Fig. 6 reveal that the geocells with "rigid walls" (HDPE and NPA) generated very similar tanδ/tanφ ratio values, particularly for both soils, with a slight decrease in efficiency observed for the NPA samples. However, the HDPE samples exhibited a frictional efficiency at least 15% higher than the NPA sample with the grout. Despite the higher surface roughness observed for Geocell C in profilometer roughness tests, the highest interface friction results were obtained for the texture pattern of the Geocell A samples, followed by Geocell B and finally Geocell C. Despite the limited scope of this experimental program, the results obtained suggest that the NPA polymer may have lower shear strength compared to the HDPE. However, further investigation is needed to confirm these preliminary results.

Lastly, Table 2 and Fig. 6 indicate that the tanδ/tanφ ratios obtained for the nonwoven geotextile geocell sample (D) were very similar to those generated by Geocell C, and slightly lower than Geocells A and B. Interestingly, DS tests determined lower tanδ/tanφ ratio values for Geocell D despite its higher roughness as determined in profilometer tests.

Influence of Cell Wall Perforations

Perforations are typically added to the walls of commercial geocells to enhance their interaction with fill materials and allow free water flow through the geocell wall. However, an excessive area of perforations may compromise the tensile strength and stiffness of the cell walls as well as the interaction with the fill material.

Figure 7 shows the results of DS tests conducted to assess the influence of the number of perforations, represented by the ratio between the sum of the perforated area (A_h), with each hole measuring 10 mm in diameter, and the cell wall area (A_w). Table 1 provides the fraction of perforation (A_h/A_w) for the geocells utilized in this research.

The results in Table 1 and in Fig. 7 indicate that the presence of 10-mm-diameter perforations in the smooth

Fig. 7 Influence of perforation fraction on tanδ/tanφ ratio

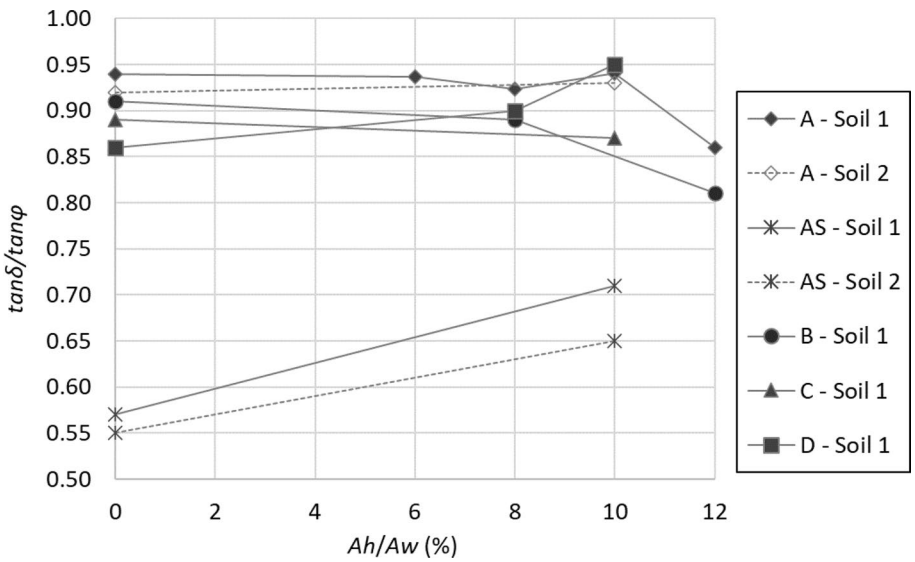

wall Geocell AS, which accounts for 10% of the total area, lead to an increase in the interface friction angle from 25° to nearly 30° for both tested soils, yielding a 20% improvement. This increase corresponds to tanδ/tanφ ratio values equal to 25 and 18%, respectively, for soil 1 and soil 2. The increase in interface shear strength can be attributed to the additional interlocking provided by the perforations (similar to that of a very high texture pattern) against the geocell wall. This interaction may also be interpreted as the passive resistance component that develops in transverse ribs of geogrids [66]. Since the Geocell AS sample is smooth, the presence of a perforation pattern of up to 10% of the specimen area generates higher surface roughness, thereby increasing its frictional efficiency and generating higher interface friction angles than the results of interface testing without perforations, regardless of soil type.

For the textured geocells with comparatively "rigid walls" (samples A, B and C), the presence of perforations, characterized by perforations fraction of 6%, 8% and 10%, did not result in significant changes in the interface friction angle and tanδ/tanφ ratio. Furthermore, the results in Fig. 7 show a slight decrease in frictional efficiency for increasing the perforation fraction from 0 to 10% of the sample area for Geocell B, particularly for soil 1, and a slight increase in the tanδ/tanφ ratio for increasing the perforation fraction from 0 to 10% of the sample area for Geocell C for the same soil. This contrasts with the trends observed for smooth wall geocells. For the textured geocell walls, the roughness pattern provides relevant interaction between the cell wall and soil. Adding perforations to the cell walls eliminates areas with high interaction, leading to a reduction in frictional efficiency and, consequently, lower interface friction angles. However, as the trend in the results in Fig. 7 reveals, the decrease in the interface friction angle for perforation fraction up to 10% was only marginal. For perforation fractions greater than 10%, there was a significant reduction in the interface friction angle and ratio of the interface friction angle to soil friction angles. Results from tests on Geocells A and B with a 12% perforation fraction for both soils indicated that only a slight decrease in the perforation fraction from 10 to 12% generates a high reduction in the tanδ/tanφ ratio—approximately 10% for both geocells walls in soil 1 (Fig. 7).

Considering that commercial geocells typically involve textured walls, the potential detrimental effect of a high number of perforations may have relevant practical implications. Specifically, the potential detrimental effects on the strength and rigidity of the cell (due to the reduced material area) as well as its frictional efficiency should be carefully evaluated. The tests conducted for this study indicated a loss of interface frictional efficiency beyond an upper limit of an approximately 10% perforated area.

Conclusions

This paper presents the results of laboratory direct shear (DS) tests conducted between geocell walls and various infill materials. Geocells from five different manufacturers, which adopted high-density polyethylene (HDPE), novel polymeric alloy (NPA) and polypropylene (PP) nonwoven geotextiles, were tested under different compaction conditions using two soil types (coarse and fine-grained soils) and grout. The testing program also involved varying the geocell wall texturing conditions and the number of perforations. Texture parameters were evaluated using a surface roughness profilometer. Analysis of the experimental results of the experimental program conducted to characterize the interface friction angles under both the peak and post-peak conditions led to the following conclusions:

- The interface friction angles obtained from tests involving textured, non-perforated geocell walls and soils were relatively high, leading to interface friction efficiency values (tanδ/tanφ) ranging from 0.83 to 0.94 for all the geocells tested in this study.
- A significant reduction in interface friction angles was observed for smooth non-perforated wall geocells, resulting in a tanδ/tanφ ratio of approximately 0.55, which represents an approximately 30% reduction in efficiency when compared to the same geocell with textured walls.
- The tanδ/tanφ ratio ranged from 0.70 to 0.97, with interface friction angles between 20° and 27°, for interfaces involving grout and geocell textured walls.
- For the geocell wall materials evaluated in this study, the large-displacement interface friction angle was slightly smaller than the value corresponding to the peak condition, resulting in reductions of approximately 10% for geocells with textured walls and no reductions for those with smooth walls.
- Perforations totaling up to 10% of the cell area were found not to compromise interface shear strength. However, increasing the perforation fraction from 10 to 12% showed a decrease in interface friction of almost 10%.
- A comparison of surface roughness profilometer results with the interface friction angles obtained from DS tests revealed that the type of texture only had a marginally influence on the frictional capacity of the geocell materials evaluated in this study. Instead, the actual presence of texture was found to be particularly significant, independent of the texturing pattern.
- Although different variables could influence the interface friction angle between the geocell walls and the infill materials, the results of this experimental program suggest that optimal frictional characteristics are achieved with textured and perforated cell walls, with a limited perforation fraction of up to 10%.

Acknowledgements The authors would like to acknowledge that the original article was supported by the São Paulo Research Foundation (FAPESP—grant #2023/04447-1) and National Council of Scientific and Technological Development (CNPq). The authors would also like to acknowledge Strata Geosystems, TDM, PRS Geo-Technologies, Ober Geosynthetics and Maccaferri for their samples.

Author Contributions J.O.A.N. conceived the research. J.C.V.Z. contributed to the implementation of the research and conducted experiments with the assistance and support by J.O.A.N. J.C.V.Z., J.O.A.N. and J.G.Z. carried out the interpretation and analysis of the results. J.O.A.N. wrote the manuscript with the support by J.G.Z. J.O.A.N. and J.G.Z. critically reviewed the manuscript for important intellectual content. J.O.A.N. supervised the project. All the authors have agreed to the content of the published version of the manuscript.

Funding No funding.

Data Availability Data are available upon reasonable request.

Declarations

Conflict of interest The authors declare no conflict of interest.

References

1. Dash SK, Choudhary AK (2018) Geocell reinforcement for performance improvement of vertical plate anchors in sand. Geotext Geomembr 46:214–225. https://doi.org/10.1016/J.GEOTEXMEM.2017.11.008
2. Mahgoub A, El NH (2020) Coupled TDA–geocell stress-bridging system for buried corrugated metal pipes. J Geotech Geoenviron Eng 146:04020052. https://doi.org/10.1061/(ASCE)GT.1943-5606.0002279
3. Song F, Liu H, Ma L, Hu H (2018) Numerical analysis of geocell-reinforced retaining wall failure modes. Geotext Geomembr 46:284–296. https://doi.org/10.1016/j.geotexmem.2018.01.004
4. Cancelli A, Rimoldi P, Montanelli F (1993) Index and performance tests for geocells in different applications. In: Cheng S (ed) Geosynthetic Soil reinforcement testing procedures. ASTM International. https://doi.org/10.1520/STP24313S
5. Richardson GN (2004) Geocells: a 25-year perspective part 1: roadway applications. Geotech Fabr Rep 22:14–19
6. Bathurst RJ, Knight MA (1998) Analysis of geocell reinforced-soil covers over large span conduits. Comput Geotech 22:205–219. https://doi.org/10.1016/S0266-352X(98)00008-1
7. Zipoli LLR, Avesani Neto JO (2022) Evaluation of back-calculated elastic moduli of unreinforced and geocell-reinforced unbound granular material from full-scale field tests. Geotext Geomembr 50:910–921. https://doi.org/10.1016/J.GEOTEXMEM.2022.05.006
8. Huang M, Lin C, Pokharel SK et al (2021) Model tests of freeze-thaw behavior of geocell-reinforced soils. Geotext Geomembr 49:669–687. https://doi.org/10.1016/J.GEOTEXMEM.2020.12.003
9. Biswas A, Murali Krishna A, Dash SK (2013) Influence of subgrade strength on the performance of geocell-reinforced foundation systems. Geosynth Int 20:376–388. https://doi.org/10.1680/gein.13.00025
10. Sitharam TG, Sireesh S, Dash SK (2005) Model studies of a circular footing supported on geocell-reinforced clay. Can Geotech J 42:693–703. https://doi.org/10.1139/t04-117
11. Tafreshi SNM, Khalaj O, Dawson AR (2014) Repeated loading of soil containing granulated rubber and multiple geocell layers. Geotext Geomembr 42:25–38. https://doi.org/10.1016/j.geotexmem.2013.12.003
12. Saride S, Baadiga R, Balunaini U, Madhira MR (2022) Modulus improvement factor-based design coefficients for geogrid- and geocell-reinforced bases. J Transp Eng Part B: Pavements 148:04022037. https://doi.org/10.1061/jpeodx.0000380
13. Madhavi Latha G, Rajagopal K (2007) Parametric finite element analyses of geocell-supported embankments. Can Geotech J 44:917–927. https://doi.org/10.1139/T07-039
14. Krishnaswamy NR, Rajagopal K, Madhavi Latha G (2000) Model studies on geocell supported embankments constructed over a soft clay foundation. Geotech Test J 23:45–54. https://doi.org/10.1520/GTJ11122J
15. Navaratnarajah SK, Indraratna B, Ngo NT (2018) Influence of under sleeper pads on ballast behavior under cyclic loading: experimental and numerical studies. J Geotech Geoenviron Eng 144:4018068. https://doi.org/10.1061/(asce)gt.1943-5606.0001954
16. Palese J, Hartsbough CM, Zarembski AM, Ling HI (2018) Field demonstration of geocell track substructure support system under high-speed passenger railroad operations DOT/FRA/ORD-18/27
17. Schary Y (2020) Case studies on geocell-based reinforced roads, railways and ports. Springer Transactions in Civil and Environmental Engineering. Springer, Singapore, pp 387–411
18. Ngo NT, Indraratna B, Biabani MM (2017) Performance assessment of geocell-reinforced subballast: modeling and design implications, pp 374–383. https://doi.org/10.1061/9780784480441.039
19. Liu Y, Deng A, Jaksa M (2018) Three-dimensional modeling of geocell-reinforced straight and curved ballast embankments. Comput Geotech 102:53–65. https://doi.org/10.1016/j.compgeo.2018.05.011
20. George AM, Banerjee A, Puppala AJ, Saladhi M (2021) Performance evaluation of geocell-reinforced reclaimed asphalt pavement (RAP) bases in flexible pavements. Int J Pavement Eng 22:181–191. https://doi.org/10.1080/10298436.2019.1587437
21. Pokharel SK, Han J, Leshchinsky D, Parsons RL (2018) Experimental evaluation of geocell-reinforced bases under repeated loading. Int J Pavement Res Technol 11:114–127. https://doi.org/10.1016/j.ijprt.2017.03.007
22. Xianrong W, Xiedong Z, Yunsheng Z, Xiaowei L (2021) Fatigue damage characteristics of geocell-reinforced asphalt mixture. Constr Build Mater 269:121252. https://doi.org/10.1016/j.conbuildmat.2020.121252
23. Baby LM, Avesani Neto JO (2024) Evaluation of geocell-reinforced railway track using FEM and FLM-based software: a parametric analysis. Int J Geosynth Ground Eng 10:64. https://doi.org/10.1007/s40891-024-00564-0
24. Bathurst RJ, Karpurapu R (1993) Large-scale triaxial compression testing of geocell-reinforced granular soils. Geotech Test J 16:296–303. https://doi.org/10.1520/gtj10050j
25. Song F, Liu H, Chai H, Chen J (2017) Stability analysis of geocell-reinforced retaining walls. Geosynth Int 24:442–450. https://doi.org/10.1680/jgein.17.00013
26. Wang GY, Liu YH, Wang XH (2012) Experimental investigation of hydrodynamic characteristics of overland flow with geocell. J Hydrodyn 24(5):737–743. https://doi.org/10.1016/S1001-6058(11)60298-9
27. Tafreshi SNM, Khalaj O, Dawson AR (2013) Pilot-scale load tests of a combined multilayered geocell and rubber-reinforced foundation. Geosynth Int 20:143–161. https://doi.org/10.1680/gein.13.00008

28. Choudhary AK, Dash SK (2021) Influence of soil density on performance of geocell-reinforced vertical anchor in sand. Geosynth Int 28:338–349. https://doi.org/10.1680/JGEIN.20.00047
29. Arvin MR, Abbasi M, Khalvati Fahliani H (2021) Shear behavior of geocell-geofoam composite. Geotext Geomembr 49:188–195. https://doi.org/10.1016/J.GEOTEXMEM.2020.09.012
30. Tavakoli Mehrjardi G, Motarjemi F (2018) Interfacial properties of Geocell-reinforced granular soils. Geotext Geomembr 46:384–395. https://doi.org/10.1016/j.geotexmem.2018.03.002
31. Manju GS, Madhavi Latha G, Rajeshkannan D (2014) Effect of pocket size on the shear properties of different sand-geocell interfaces. In: 10th international conference on geosynthetics, ICG 2014, pp 1285–1292
32. Isik A, Gurbuz A (2020) Pullout behavior of geocell reinforcement in cohesionless soils. Geotext Geomembr 48:71–81. https://doi.org/10.1016/J.GEOTEXMEM.2019.103506
33. Khedkar MS, Mandal JN (2009) Pullout behaviour of cellular reinforcements. Geotext Geomembr 27:262–271. https://doi.org/10.1016/j.geotexmem.2008.12.003
34. Fakharian K, Pilban A (2021) Pullout tests on diagonally enhanced geocells embedded in sand to improve load-deformation response subjected to significant planar tensile loads. Geotext Geomembr 49:1229–1244. https://doi.org/10.1016/J.GEOTEXMEM.2021.04.002
35. Khalaj O, Moghaddas Tafreshi SN, Mašek B, Dawson AR (2015) Improvement of pavement foundation response with multi-layers of geocell reinforcement: cyclic plate load test. Geomech Eng 9:373–395. https://doi.org/10.12989/gae.2015.9.3.373
36. Garcia RS, Avesani Neto JO (2021) Stress-dependent method for calculating the modulus improvement factor in geocell-reinforced soil layers. Geotext Geomembr 49:146–158. https://doi.org/10.1016/j.geotexmem.2020.09.009
37. Ari A, Misir G (2021) Three-dimensional numerical analysis of geocell reinforced shell foundations. Geotext Geomembr 49:963–975. https://doi.org/10.1016/J.GEOTEXMEM.2021.01.006
38. ABNT NBR 7214 (2015) Standard sand for cement tests - Specification. 4
39. ASTM D3080 (2011) Standard test method for direct shear test of soils under consolidated drained conditions
40. Potyondy JG (1961) Skin friction between various soils and construction materials. Géotechnique 11:339–353. https://doi.org/10.1680/geot.1961.11.4.339
41. Zornberg JG, McCartney JS, Swan RH (2005) Analysis of a large database of gcl internal shear strength results. J Geotech Geoenviron Eng 131:367. https://doi.org/10.1061/(asce)1090-0241(2005)131:3(367)
42. McCartney JS, Zornberg JG, Swan RH (2009) Analysis of a large database of GCL-geomembrane interface shear strength results. J Geotech Geoenviron Eng 135:209. https://doi.org/10.1061/(asce)1090-0241(2009)135:2(209)
43. Vaid YP, Rinne N (1995) Geomembrane coefficients of interface friction. Geosynth Int 2:309. https://doi.org/10.1680/gein.2.0012
44. Benjamim CVS, Bueno BS, Zornberg JG (2007) Field monitoring evaluation of geotextile-reinforced soil-retaining walls. Geosynth Int 14:100–118. https://doi.org/10.1680/gein.2007.14.2.100
45. Brink G (2015) A brief overview of the typical engineering characteristics of tropical red soils. In: Engineering geology for society and territory— volume 6: applied geology for major engineering projects. Springer International Publishing, pp 211–214
46. Ehrlich M, Silva RC (2015) Behavior of a 31 m high excavation supported by anchoring and nailing in residual soil of gneiss. Eng Geol 191:48–60. https://doi.org/10.1016/j.enggeo.2015.01.028
47. Northmore KJ, Culshaw MG, Hobbs PRN (1992) Engineering geology of tropical red clay soils: summary findings and their application for engineering purposes. Technical report WN/93/15. British Geological Survey, Keyworth/Nottingham
48. Santos OF, Lacerda WA, Ehrlich M (2020) Effects of cyclic variations of pore pressure on the behaviour of a gneiss residual soil. Geotech Geol Eng 38:5201–5212. https://doi.org/10.1007/s10706-020-01356-9
49. Tuncer ER, Lohnes RA (1977) An engineering classification for certain basalt-derived lateritic soils. Eng Geol 11:319–339. https://doi.org/10.1016/0013-7952(77)90037-0
50. Vargas M (1953) Some engineering proprieties of residual clay soils occouring in Southern Brazil. In: 3rd international conference on soil mechanics and foundation engineering, Zurich, pp 67–71
51. Vargas M (1973) Structurally unstable soils in Southern Brazil. In: 8th international conference on soil mechanics and foundation engineering, Moscow, pp 239–246
52. Portelinha FHM, Goulart JMH, Avesani Neto JO (2023) Influence of heterogeneous arrangements of reinforcements' length and stiffness on the deformation of instrumented geosynthetic-reinforced retaining walls constructed with sustainable locally available backfill soils. Sustainability (Switzerland) 15:8183. https://doi.org/10.3390/su15108183
53. ISO 4287 (1997) Geometrical product specifications (GPS)—surface texture: profile method—terms, definitions and surface texture parameters
54. Hamidi A, Garousi AH (2024) Effect of particle size on the anisotropic shear behavior of sand-textured geomembrane interface. In: Proceedings of the institution of civil engineers: ground improvement. https://doi.org/10.1680/jgrim.23.00014
55. Araújo GLS, Sánchez NP, Palmeira EM, de Almeida MDGG (2022) Influence of micro and macroroughness of geomembrane surfaces on soil-geomembrane and geotextile-geomembrane interface strength. Geotext Geomembr 50:751. https://doi.org/10.1016/j.geotexmem.2022.03.015
56. Ingold TS (1990) Friction testing—geomembranes: identification and performance testing. CRC Press, Boca Raton
57. O'Rourke TD, Druschel SJ, Netravali AN (1990) Shear strength characteristics of sand-polymer interfaces. J Geotech Eng 116:451–469. https://doi.org/10.1061/(ASCE)0733-9410(1990)116:3(451)
58. Koerner RM (1994) Designing with geosynthetics. 1st edn. Prentice Hall, New Jersey
59. Sharma HD, Lewis SP (1994) Waste containment systems, waste stabilization, and landfills: design and evaluation. Wiley, Hoboken
60. Izgin M, Wasti Y (1998) Geomembrane-sand interface frictional properties as determined by inclined board and shear box tests. Geotext Geomembr 16:207–219. https://doi.org/10.1016/S0266-1144(98)00010-7
61. Pitanga HN, Gourc JP, Vilar OM (2009) Interface shear strength of geosynthetics: evaluation and analysis of inclined plane tests. Geotext Geomembr 27:435–446. https://doi.org/10.1016/j.geotexmem.2009.05.003
62. Aldeeky H, Al Hattamleh O, Alfoul BA (2016) Effect of sand placement method on the interface friction of sand and geotextile. Int J Civ Eng 14:133–138
63. Choudhary AK, Krishna AM (2016) Experimental investigation of interface behaviour of different types of granular soil/geosynthetics. Int J Geosynth Ground Eng 2:1–11. https://doi.org/10.1007/s40891-016-0044-8
64. Santos DAM, Kamiji TSMM, Plácido RR, Avesani Neto JO (2010) Reflections about interface strength between soils and textured geomembranes. In: 9th international conference on geosynthetics. Guarujá
65. Junior SLDC, Aparicio-Ardila MA, Palomino CF, Lins da Silva J (2023) Analysis of textured geomembrane-soil interface strength

to mining applications. Int J Geosynth Ground Eng 9:3. https://doi.org/10.1007/s40891-022-00423-w
66. Jewell RA, Milligan GWE, Sarsby RW, Dubois D (1984) Interaction between soil and geogrids. In: conference on polymer grid reinforcement in civil engineering. pp 18–30
67. Lopes PC, Lopes ML, Lopes MP (2001) Shear behaviour of geosynthetics in the inclined plane test—influence of soil particle size and geosynthetic structure. Geosynth Int 8:327–342. https://doi.org/10.1680/gein.8.0198